Cooperative Interactions of the Catalytic Nucleophile and the Catalytic Acid in the Inhibition of β-Glycosidases. Calculations and Their Validation by Comparative Kinetic and Structural Studies of the Inhibition of Glycogen Phosphorylase *b*

by **Tom D. Heightman**[a]), **Andrea Vasella**[a])*, **Katerina E. Tsitsanou**[b]), **Spyros E. Zographos**[b]), **Vicky T. Skamnaki**[b]), and **Nikos G. Oikonomakos**[b])*

[a]) Laboratory of Organic Chemistry, ETH-Zentrum, Universitätstrasse 16, CH-8092 Zürich
[b]) Institute of Biological Research and Biotechnology, National Hellenic Research Foundation, 48 Vas. Constantinou Avenue, Athens 11635, Greece

The difference between the strong inhibition of retaining β-glucosidases by the tetrazole **1** and the weak inhibition by the triazole **3** has been explained by the protonation by the enzymic catalytic acid of N(3) of **1**, replaced by CH in **3**. One also expects a contribution to the inhibition from the charge-dipole interaction between the enzymic catalytic nucleophile and the azole ring. The extent of this contribution was estimated from the calculated, distance-dependent heats of formation of the acetate-azole complexes. The calculations were validated by comparison of the charge-dipole interaction between phosphate and the inhibitors **1** and **3** in the glycogen phosphorylase *b* (GP*b*)-azole-phosphate complexes, as derived from differences in the K_i values for **1** and **3**, while the structural invariance of the complexes was demonstrated by X-ray analysis. The difference between the charge-dipole interactions of (dihydrogen)phosphate and **1** or **3** as derived from ΔK_i is 1.1 kcal mol^{-1}, while the calculated difference is 1.3 kcal mol^{-1}. The calculated difference for the interaction of **1** or **3** with acetate, representing the catalytic nucleophile in β-glycosidases, is 2.0 kcal mol^{-1}, while the differences of the binding energies as derived from the K_i values for the inhibition by **1** or **3** of different β-glycosidases range from 2.4 to 5.3 kcal mol^{-1}. The calculated difference for **1** and the imidazole **6** is 2.5 kcal mol^{-1} in favour of **1**, whereas the K_i-derived difference is 3.7 kcal mol^{-1} in favour of **6**, equal to the calculated difference between **1** and the protonated imidazole **6**. Thus, protonation by the catalytic acid and the charge-dipole interaction with the catalytic nucleophile contribute cooperatively to the binding of inhibitors possessing a trigonal anomeric centre bonded to a heteroatom.

Introduction. – The observation that the *gluco*-tetrazole **1** and the 1,2,4-triazole **2**, but not the isomeric 1,2,3-triazole **3**, are strong competitive inhibitors of several retaining β-glucosidases is relevant to a detailed understanding of the inhibition of glycosidases by transition-state analogues, and thus of the mechanism of action of these enzymes [1–4]. The inhibition of β-glycosidases by the azoles **1**, **2**, or **3** correlates with the presence or absence of an N-atom (N(1) of **1**) corresponding to the glycosidic (= anomeric) O-atom (*cf. Fig. 1*) [1–4]. The differences have been rationalized by postulating that a partial proton transfer from the catalytic acid (AH) to the doubly occupied, nonbonding orbital of N(1) is a prerequisite for strong inhibition [1].

Given the transition-state-analogue character of the tetrazole **1**[1]) and most probably of the triazole **2**, H-bond donation to these inhibitors and protonation of the substrate in the course of the enzyme-catalysed reaction should be similar to each other. Since these inhibitors can only be protonated in the plane of the ring, but not perpendicularly to it,

[1]) As shown for the *Agrobacterium faecalis* β-glucosidase [5].

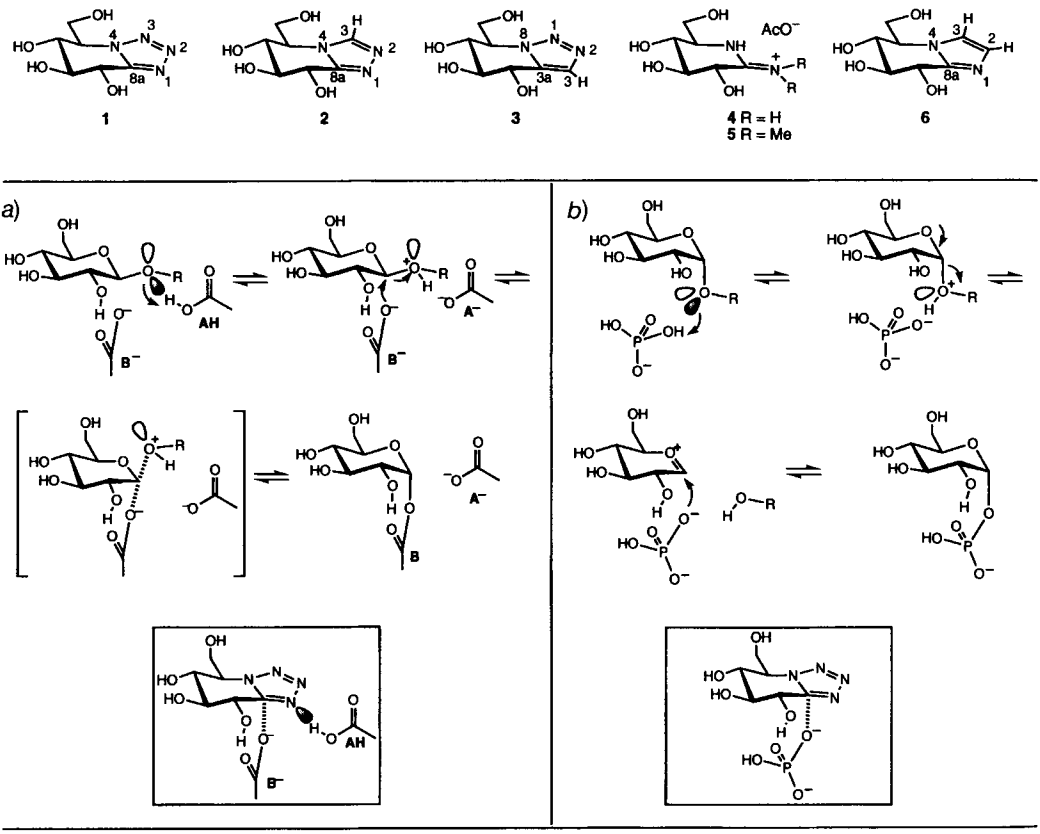

Fig. 1. *Transition-state analogue inhibitors of β-glycosidases showing the numbering system used, with the mechanism and inhibition by* **1** *of* a) *retaining β-glycosidases and* b) *glycogen phosphorylase* b

the same should be valid for the substrates of those retaining β-glycosidases that are strongly inhibited by **1** and **2**, and (by extrapolation) analogous inhibitors possessing an sp^2-hybridized heteroatom at the anomeric centre, but not by related compounds lacking this heteroatom (*Fig. 1,a*) [1]. This implies that the catalytic proton donor must be located close to the mean plane of the pyranoside ring. This has now been confirmed by the crystal structures of several glycosidase-ligand complexes [6–8].

Partial proton transfer, however, cannot be a factor in the inhibition of retaining β-glycosidases by permanently charged inhibitors, such as the amidinium acetates **4** and **5** [9]; charge-charge interaction with the catalytic nucleophile (B^-) must be responsible for the inhibition by such salts.

This raises the questions to which extent a charge-dipole interaction between the catalytic nucleophile B^- and an azole contributes to the inhibition and hence to the differences in the inhibition by **1** and **2** *vs.* **3**, and to which extent partial protonation of **1**, **2**, and the related imidazole **6** [4][10] enhances the charge-dipole interaction with B^-, ultimately transforming it into a charge-charge interaction. Such a cooperative effect between H-bonding and the interaction with the catalytic nucleophile could explain the

increasing strength of the inhibition of several glucosidases by the tetrazole **1**, the triazole **2**, and the imidazole **6**, and similarly of related mannosidases and galactosidases by the corresponding diastereoisomeric azoles (*cf. Table 1*) [5][11].

Table 1. *Inhibition of Sweet Almond β-Glucosidase and Glycogen Phosphorylase* b (GP*b*) *by the Azole Inhibitors* **1**–**3** *and* **6**

Inhibitor	K_i(β-glucosidase)/μM	K_i(GP*b*/phosphate)/μM	K_i(GP*b*/Glc1*P*)/μM
1	150[a]) [3]	53[b]) [9]	700[a]) [9]
2	19[a]) [5]	8100[b])	–[d])
3	> 8000[c]) [2]	540[b])	2500[a])
6	0.35[a]) [4]	9700[b])	–[d])

[a]) Competitive. [b]) Uncompetitive. [c]) No inhibition. [d]) No inhibition at concentrations of inhibitors varied from 0.1 to 5 mM in the presence of 3 mM Glc1*P*, 1 mM AMP, and 1% of glycogen.

We wished to learn about the energy of such a charge-dipole interaction, and about the extent to which it is enhanced by H-bonding to the azole ring. This energy may be calculated, but in view of the uncertainty regarding the dielectric constant in the active site, such calculations need to be validated. For this, we planned to refer to the similar charge-dipole interaction that has been postulated to occur between the tetrazole **1** and a (hydrogen- or dihydrogen)phosphate to explain the observation that **1** inhibits glycogen phosphorylase *b* (GP*b*)[2]) much more strongly in the presence of phosphate (K_i = 53 μM) than in its absence (K_i = 700 μM) (*cf. Fig. 1,b*) [12]. We intended to compare calculations of the charge-dipole interaction between the phosphate group and **1** or **3** bound to GP*b* with kinetic data on the inhibition and with structural information. This should validate the calculations and confer a reasonable degree of confidence to similar calculations, using acetate in place of phosphate, to learn about the charge-dipole interaction in retaining β-glycosidases. A comparison of the action of a retaining β-glucosidase and GP*b* indeed shows that the formation of the C(1)–O bond leading to a glucosyl phosphate (*Fig. 1,b*) is similar to the formation of the C(1)–O bond leading to the glycosyl ester (*Fig. 1,a*). X-Ray analysis of the ternary complex [GP*b*-tetrazole **1**-phosphate] has shown a close contact (3.1 Å) between the proximal O-atom of the phosphate residue and the 'anomeric' C-atom (C(8a)) of **1** [12] (*cf. Fig. 1,b*)[3]). Moreover, the complex shows clearly that there is no amino-acid side chain corresponding to the proton donor in β-glycosidases and, therefore, no H-bond donation to the N-atom in the 'glycosidic' position of the inhibitor[4]). Thus, the GP*b* complex provides a model system

[2]) Abbreviations: GP, glycogen phosphorylase, 1,4-α-D-glucan:orthophosphate α-glucosyltransferase (EC 2.4.1.1); GP*b*, glycogen phosphorylase *b*; GP*a*, glycogen phosphorylase *a*; PLP, pyridoxal 5'-phosphate; Glc1*P*, α-D-glucose 1-phosphate; UDP-Glc, uridine 5'-diphosphate α-D-glucose; heptulose-2-*P*, 1-deoxy-D-*gluco*-heptulose 2-phosphate; BES, *N,N*-bis(2-hydroxyethyl)-2-aminoethanesulfonic acid; DTT, dithiothreitol; r.m.s., root-mean-square.

[3]) The arrangement of the phosphate anion and the tetrazole is structurally very similar to the arrangement between the catalytic nucleophile and the substrates or inhibitors proposed in our models [1] and confirmed by crystal-structure analyses by other groups [6–8].

[4]) This is in keeping with the evidence that, for the cleavage of glycogen by GP*b*, phosphate plays both the roles of the catalytic acid and of the catalytic nucleophile, and that no acidic function of the enzyme is directly involved in the protonation of glycogen [13][14].

in which differences in the charge-dipole interactions for **1**, **2**, **3**, and **6** can be investigated in the absence of differences in the enzyme-azole-N(1) H-bonding.

We now report the results of the energy calculations for the charge-dipole interactions between hydrogen- or dihydrogenphosphate and the tetrazole **1**, the isomeric triazoles **2** and **3**, and the imidazole **6**, the validation of these calculations, and the results of similar calculations using a carboxylate anion in place of phosphate.

Results and Discussion. – *Kinetic Studies.* Triazole **3** acts as an uncompetitive inhibitor of the enzyme with respect to phosphate, with a K_i value of 540 μM. *Lineweaver-Burk* plots of the kinetic data for the inhibition of GP*b* by **3** in the presence of varying concentrations of phosphate, assayed in the direction of glycogen breakdown, are shown in *Fig. 2*. The compound is 10 times less effective than the tetrazole **1** (K_i = 53 μM) [12]. Competitive inhibition was observed when GP*b* was assayed in the direction of glycogen synthesis, with varying concentrations of Glc1*P*. A K_i of 2.5 mM was obtained. Uncompetitive inhibition was also observed with the azole inhibitors **2** and **6**, with K_i values more than 10 times higher than that of the triazole **3** (*Table 1*). The difference in binding energy ΔE_b as derived from the difference between the K_i values of the tetrazole **1** and the 1,2,3-triazole **3** thus amounts to 1.3 kcal mol^{-1}.

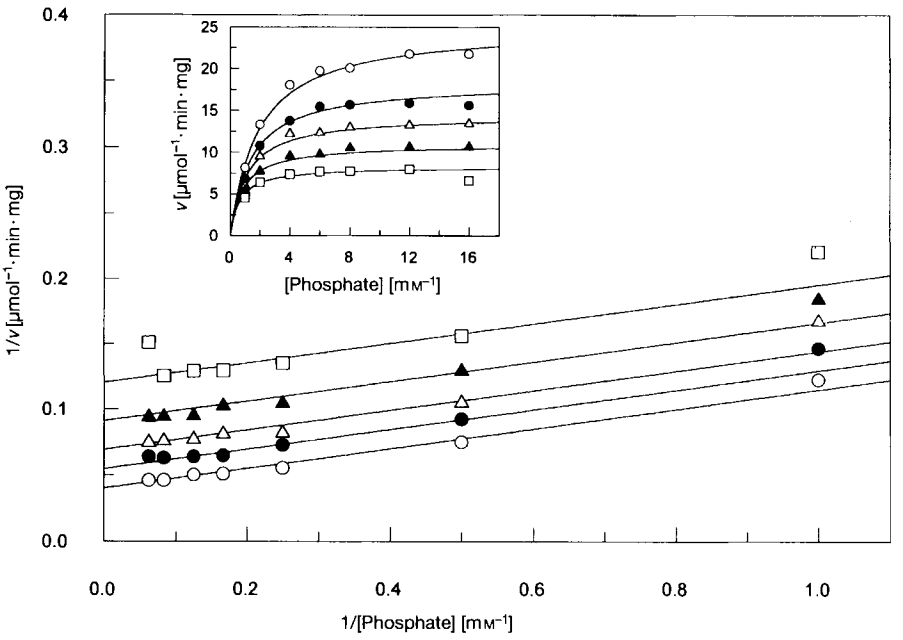

Fig. 2. *Kinetics of triazole* **3** *inhibition of GP*b *with respect to phosphate in the direction of glycogen breakdown: Double reciprocal plots of initial reaction velocity* vs. *phosphate* (1, 2, 4, 6, 8, 12, and 16 mM) *at constant concentrations of AMP* (1 mM) *and glycogen* (0.5%). Triazole concentrations were as follows. 0 (○), 0.2 (●), 0.4 (△), 0.7 (▲), and 1.1 mM (□). Best fit lines were computer-generated according to the equation for uncompetitive inhibition (GraFit) by fitting all of the data at once. The kinetic parameters determined by this method are as follows: K_m = 1.88 ± 0.12 mM, v_{max} = 25.0 ± 0.5 μmol/min/mg, K_i = 0.54 ± 0.02 mM. *Inset*: Fit of the calculated lines to the initial rate measurements.

The weak, uncompetitive inhibition of GP*b* by the 1,2,4-triazole **2** and the imidazole **6** shows that they do not interact significantly with the active site of this enzyme. Both azoles have CH in the position of N(1) of **3** (equivalent to N(3) of **1**), which makes close contact with Leu-136 (a H-bond to the backbone NH, and *van der Waals* contacts with the isopropyl side chain) in the crystal structures of the [GP*b*-tetrazole-phosphate] and [GP*b*-triazole **3**-phosphate] complexes (see below; *cf. Fig. 3*). Therefore, the inhibition of GP*b* by **2** and **6** was not considered for the validation of the calculations.

Crystallographic Studies. The crystal structure of the [GP*b*-triazole-phosphate] complex at 2.3-Å resolution[5]) shows that the triazole and phosphate are bound at the catalytic site, consistent with the kinetic observations. The triazole fits neatly into the catalytic site, and the inhibitor exploits numerous contacts (*Fig. 3*). The conformation of the triazole is close to that observed in the uncomplexed triazole single-crystal structure [1].

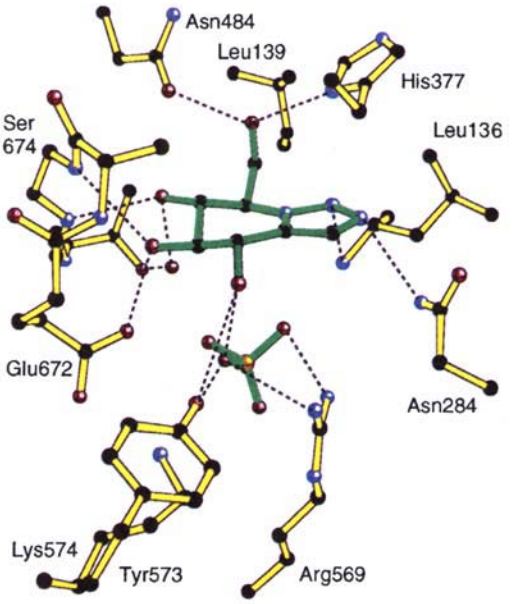

Fig. 3. *Contacts between the triazole* **3**, *phosphate, and enzyme groups at the catalytic site of T state GP*b

Comparison of the structure of the [GP*b*-triazole-phosphate] complex with that of the room temperature [GP*b*-tetrazole-phosphate] structure (2.4 Å) (*PDB* code: 1NOJ) and of the 100-K [GP*b*-tetrazole-phosphate] structure (1.7 Å) (*PDB* code: 1NOK) [12] shows that the positions of the Ca-atoms (excluding mobile regions with *B* factors greater than 60 Å^2) deviate from their mean positions by 0.375 and 0.326 Å, respectively, indicating that these complexes are quite similar in their overall conformation within the limits of the 2.3 Å resolution. In particular, in the [GP*b*-triazole-phosphate] complex, the

[5]) Coordinates have been deposited with the *Protein Data Bank*, Brookhaven National Laboratory, Upton NY 11973 (*PDB* ID code: 1AXR).

280s loop, Arg-569, and His-571 are almost in the same position as in the [GP*b*-tetrazole-phosphate] complex. A comparison of the position of the triazole **3**/phosphate and the tetrazole **1**/phosphate at the catalytic site is shown in *Fig. 4*. The atoms of these complexes are almost exactly superimposed. In other words, the replacement of N(3) of the tetrazole **1** by CH has no significant effect on the structure of the enzyme in the complex at the 2.3-Å resolution (estimates of the precision of coordinates taken from previous studies indicate errors of the order of 0.2 Å [15]).

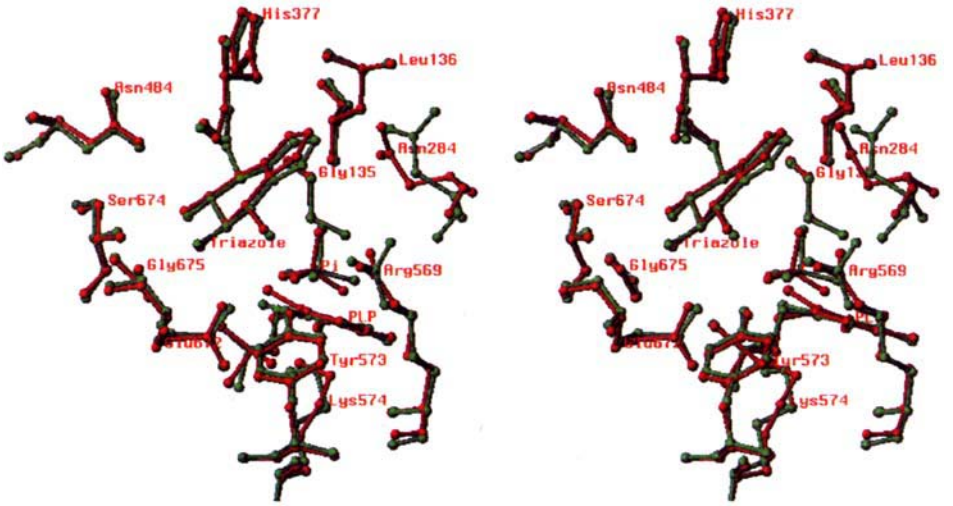

Fig. 4. *Comparison between the T-state [GP*b*-triazole-phosphate]* (red) *and the T-state [GP*b*-tetrazole-phosphate]* (green) *complexes at the catalytic site*

Previous X-ray crystallographic studies on muscle glycogen phosphorylase have led to a detailed description of the catalytic, nucleoside, and allosteric sites [16–18]. The catalytic site is located at the centre of the molecule, *ca.* 12 Å from the surface, and close to the essential pyridoxal-phosphate cofactor. Access to the catalytic site is *via* a channel, and in the T state, the channel is partly blocked by the 280s loop. Conversion of the T-state GP*b* to the R state results in several changes at the catalytic site, which include a displacement of the 280s loop (residues 282–286) that allows access to the catalytic site and the replacement of Asp-283 by Arg-569. The nucleoside inhibitor site is located at the entrance to the catalytic-site channel some 12 Å from the catalytic site. Ligands which bind at this site (*e.g.*, aromatic compounds such as caffeine) intercalate between the aromatic side chains of Phe-285 and Tyro-13 and partially block access to the catalytic site. Binding at this site stabilizes the geometry of the 280s loop occurring in the T state. No triazole was bound at this site, consistent with previous results which suggest that substrate Glc1*P*-like inhibitors such as UDP-Glc or heptulose-2-*P* promote the R-state conformation of the enzyme by causing disruption of the nucleoside inhibitor binding site, since the 280s loop, containing Phe-285, must move to accommodate substrates or R state substrate analogues [19][20]. The allosteric site is situated at the subunit-subunit interface of the dimeric molecule and is some 30 Å from the catalytic site. The site, which

is composed of 2 arginine residues, Arg-309 and Arg-310, and a more distant arginine, Arg-242, recognizes a variety of phosphorylated compounds (such as AMP, IMP, ATP, Glc6*P*, NADH, and inorganic phosphate) that may either activate by promoting the R state or inhibit by promoting the T state.

There is little overall conformational change in the tertiary structure of GP*b* on binding the triazole and phosphate. The r.m.s. difference in Ca-atoms with respect to the 100-K native GP*b* structure (2.0 Å) with MPD used as a cryoprotectant (*Gregoriou et al.*, unpublished results) is 0.314 Å if those residues that are mobile with *B* factors > 60 Å^2 are omitted. Although this value is small, there are large local conformational changes that represent the changes upon the T to R transition. The major conformational changes on binding the triazole and phosphate occur in the vicinity of the catalytic site. Thus, the 280s loop, which blocks access to the catalytic site in the T state, alters its conformation resulting in substantial rearrangements in the side chains of Asp-283 and Asn-284. Arg-569 occupies the position close to that occupied by Asp-283 in the T state, and the interchange between an acidic and a basic group helps to create the substrate phosphate recognition site. His-571, which, in the native enzyme, makes contact with the 280s loop through Asp-283, shifts to make a H-bond to the newly positioned side chain of Asp-283.

Phosphate was also found at the allosteric effector recognition site. In the [GP*b*-triazole-phosphate] complex, Arg-309 shifts its side-chain conformation to make the contact with the phosphate, a shift that is also observed on binding phosphorylated compounds. The interactions between phosphate and the phosphorylase allosteric effector site are dominated by charge-charge interactions between the phosphate group and arginine residues Arg-309 and Arg-310 (data not shown). At the allosteric site, there are no other significant differences in amino-acid side-chain positions, and the residues remain in their T-state conformation.

Semi-Empirical Calculations. The interactions between each inhibitor (**1**, **2**, **3**, or **6**) and a phosphate ion (see below) were modelled semi-empirically using AM1 [21]. Initial minimization of each inhibitor alone gave structures in close agreement with the X-ray analyses of the tetrazole **1** [2], 1,2,3-triazole **3** [1], and imidazole **6** [4]. The calculated LUMO energies[6]) of the azoles **1**, **2**, **3**, and **6** follow the expected sequence (*Table 2*). For each azole, the largest coefficient of the LUMO is at the 'anomeric' C-atom (C(8a) for **1** and **2**; C(3a) for **3**), except for the imidazole, for which the coefficients of the LUMO are approximately equal for C(3) and C(8a). The potential energy for the interaction between phosphate and the inhibitor was simulated by reducing the distance between the proximal phosphate O-atom and the 'anomeric' C-atom (O···C('anomeric')) by increments of 0.1 Å, and determining the heat of formation of each complex (see *Fig. 5*). In the enzyme, the phosphate ion is involved in a number of H-bonds and electrostatic interactions which partially neutralize the negative charge. To reproduce this situation as closely as possible, the phosphate was modelled as either a hydrogenphosphate or a dihydrogenphosphate ion. In each case, a minimum of constraints were imposed on the system, such that the H-bond between HO–C(2) (carbohydrate nomenclature) of the inhibitor and the phosphate was conserved, and the proximal phosphate O-atom approached the 'anomeric' C-atom perpendicularly to the ring plane of the inhibitor, as observed in the crystal structures of the ternary complexes [GP*b*-tetrazole **1**-phosphate]

[6]) The energy of the charge-dipole interaction is expected to correlate with the energy of the LUMO.

and [GP*b*-triazole **3**-phosphate]. The energy of the interactions between either hydrogenphosphate or dihydrogenphosphate and each inhibitor is characterized by a typical *Lennard-Jones* potential (*Fig. 5,a* and *b*; *Table 2*). Since the resulting potential-energy curves are derived from differing heats of formation, they were normalized to zero at distance O···C('anomeric') of 4.0 Å to allow a comparison of the interaction energies of the inhibitors.

Table 2. *Results of AM1 Calculations for the Charge-Dipole Interaction between* HPO_4^{2-}, $H_2PO_4^-$, *or* $CH_3CO_2^-$ *and the Azole Inhibitors* **1**–**3** *and* **6**

Inhibitor	E_{LUMO}/kcal mol^{-1}	HPO_4^{2-}		$H_2PO_4^-$		$CH_3CO_2^-$	
		E_{min} [a])	ΔE_c [b])	E_{min} [a])	ΔE_c [b])	E_{min} [a])	ΔE_c [b])
1	−0.298	−8.6 (2.7)	0	−2.8 (3.1)	0	−4.6 (2.6)	0
2	0.156	−7.8 (3.0)	+0.8	−2.0 (3.2)	+0.8	−3.0 (2.8)	+1.6
3	0.111	−6.6 (3.0)	+2.0	−1.7 (3.2)	+1.1	−2.6 (2.9)	+2.0
6	0.788	−5.9 (3.1)	+2.7	−1.1 (3.4)	+1.7	−2.1 (3.0)	+2.5
6 · H^+	−4.492	–	–	–	–	−8.3 (2.7)	−3.7

[a]) Values in parentheses give the distance in Å between the proximal O-atom and the 'anomeric' C-atom at E_{min}.
[b]) ΔE_c gives the difference between the energy minima (E_{min}) of **1** and the other azoles.

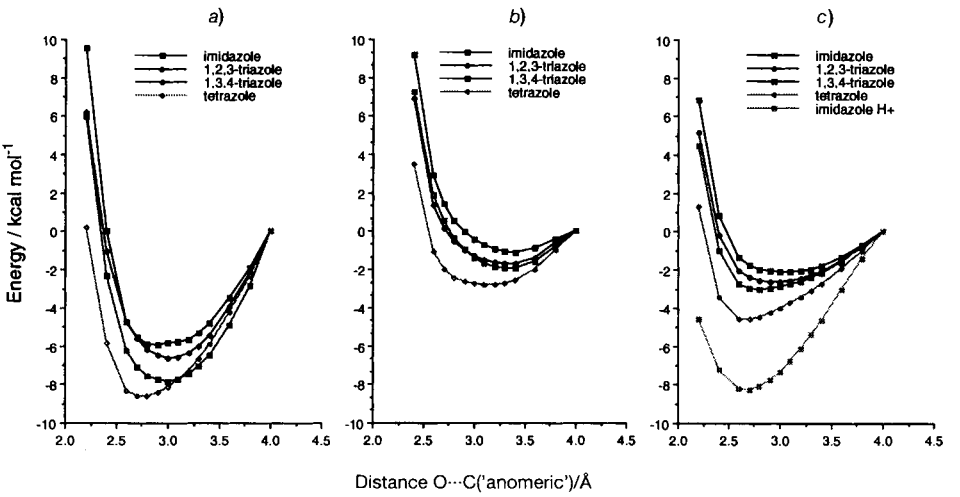

Fig. 5. *Plots of potential energy against the distance between the proximal O-atom and the 'anomeric' C-atom for* a) HPO_4^{2-}, b) $H_2PO_4^-$, *and* c) $CH_3CO_2^-$ *and the indicated azole inhibitors* **1**, **2**, **3**, *and* **6**

With dihydrogenphosphate, the energy minimum (E_{min}) occurs at distance O···C('anomeric') of 3.1 Å for the tetrazole **1**, at 3.2 Å for the triazoles **2** and **3**, and at 3.4 Å for the imidazole **6**. With hydrogenphosphate, the tetrazole **1** shows its strongest interaction at 2.7 Å, the triazoles **2** and **3** at 3.0 Å, and the imidazole **6** at 3.1 Å. The distance O···C('anomeric') of 3.1–3.2 ± 0.2 Å for **1** and **3** in the two X-ray structures is hence better reproduced at the energy minima of the dihydrogenphosphate potential-energy curves. Among the inhibitors **1**–**3** and **6**, the tetrazole **1** shows the strongest

interaction with either hydrogen- or dihydrogenphosphate. The 1,2,4-triazole **2** shows similar behaviour to the 1,2,3-triazole **3**. The weakest interaction energy both with hydrogen- and with dihydrogenphosphate is found for the imidazole **6**.

The difference of binding energy ΔE_b (1.3 kcal mol^{-1}, see above) is approximately equal to the difference ΔE_c of 1.1 kcal mol^{-1} obtained by subtracting the two dihydrogenphosphate potential-energy curves[7]) for the interaction of phosphate with the inhibitors **1** and **3**. As the two inhibitors are bound in the same way (within the limits of the resolution), the difference in binding energy ΔE_b should be equal to the calculated ΔE_c. The difference between the two ΔE values is within the limits of the level of the calculation and of the precision of the kinetic measurements. We conclude that the calculations yield significant results.

Under the same geometric constraints, the interactions between each inhibitor and the carboxylate nucleophile of β-glycosidases were modelled using an acetate ion in place of phosphate. A similar energy-distance relation for the charge-dipole interaction is observed (*Fig. 5,c*). The potential-energy minimum occurs at 2.6 Å for the tetrazole **1**, and at 2.8–3.0 Å for the triazoles **2** and **3** and the imidazole **6**. Among the neutral azoles, the interaction energy is again strongest for the tetrazole **1** and weakest for the imidazole **6**; ΔE_c for the tetrazole **1** and the triazole **3** is 2.0 kcal mol^{-1}. This compares with differences in β-glycosidase binding energies ΔE_b of 2.4–5.3 kcal mol^{-1} for **1** and **3** and their *manno*-diastereoisomers [1]. Thus, the charge-dipole interaction accounts for some but not all of the difference in binding affinity.

The calculated difference ΔE_c for the tetrazole **1** and imidazole **6** is 2.5 kcal mol^{-1} in favour of **1**, but the difference in binding energy ΔE_b is 3.7 kcal mol^{-1} in favour of **6** (*Table 1*, [4]), which means that H-bonding must play a major role in the binding of **6**. Indeed, protonation of the imidazole **6** considerably lowers its LUMO (by over 4 kcal mol^{-1}), and the interaction of acetate with the imidazolium cation is 3.7 kcal mol^{-1} stronger than with the neutral **1**. This evidences the cooperative effect on the inhibition of the H-bond between N(1) and the catalytic acid (AH) of the glycosidase, and the charge-dipole (charge-charge) interaction between the inhibitor and the catalytic nucleophile (B^-), as depicted in *Fig. 1,a*. In other words, the stronger the H-bonding interaction with AH in the σ-plane of the azole, the more the LUMO energy is lowered, and the stronger becomes the charge-dipole interacton with B^- in the π-plane. This means that, for β-glycosidases, the K_i values cannot be taken as a measure of the individual contributions of the proton transfer and the dipolar interaction.

The azolopyridine inhibitors have thus allowed enzyme-inhibitor interactions to be delineated by systematic variation of the strength of the H-bond (including its elimination) between the catalytic acid and the inhibitor. The combined interactions are likely to be responsible for the binding of other inhibitors with a trigonal anomeric C-atom bonded to a heteroatom, such as glyconolactones [22], the related lactams [23] and hydroximolactams [24][25], and other analogues.

We wish to acknowledge the assistance of the staff at *ELETTRA*, Trieste, Italy, in X-ray data collection, Prof. *L. N. Johnson* for critical advice, and the final year project students *S. Avlonites* and *D. Katharios* for contributions to the kinetic experiments. This work was supported by the *Swiss National Science Foundation* and *F. Hoffmann-La Roche Ltd.*, Basel (*T.D.H.* and *A.V.*) and the Greek GSRT (PENED-225) and EU contract ERB FMGE CT95 0022 through minor grant 209/96 (*N.G.O.*).

[7]) As compared to 2.0 kcal mol^{-1} for the hydrogenphosphate curves.

Experimental Part

General. AMP, Glc1*P* (dipotassium salt), glycogen, NADP, glucose-6-*P* dehydrogenase, glucose 1,6-diphosphate, and other chemicals were obtained from *Sigma Chemical Co.* Oyster glycogen was freed of AMP by the method of *Helmreich* and *Cori* [26]. Rabbit phosphoglucomutase, purchased from *Sigma* as a suspension in 2.5M ammonium sulfate, was dialysed against 60 mM β-glycerophosphate, 4.5 mM EDTA, 3 mM DTT buffer (pH 6.8) just before use. Glycogen phosphorylase *b* was isolated from rabbit skeletal muscle according to *Fischer* and *Krebs* [27] using 2-mercaptoethanol instead of L-cysteine, and recrystallized at least 4 times. Bound nucleotides were removed from the enzyme as described [28]. Protein concentration was determined from absorbance measurements at 280 nm using an absorbance index $A^{1\%}_{1\,cm} = 1.32$ [29].

Kinetic Studies. Phosphorylase activity in the direction of glycogen breakdown was carried out using the auxiliary assay system as described by *Helmreich* and *Cori* [26] with some modifications. The final reaction mixtures were 0.3 ml and contained phosphorylase *b* (1.2 µg), glucose-6-phosphate dehydrogenase (4 µg), phosphoglucomutase (10 µg), 1 mM NADP, 1 µM glucose 1,6-diphosphate, 20 mM 1*H*-imidazole, 2.4 mM β-glycerophosphate, 10 mM 2-mercaptoethanol, 0.3 mM EDTA, 0.1 mM DTT, 10 mM magnesium acetate, 1 mM AMP, 0.5% of glycogen, and a range of concentrations of phosphate and inhibitors (pH 6.8 and 30°). Enzyme, AMP, and glycogen were preincubated for 15 min at 30°, before the reaction was initiated by adding the above mixture. The reaction was stopped by addition of sodium dodecyl sulfate to reach a final concentration of 0.1%, at times selected to secure linearity of the assay. NADPH formed in the reaction was measured at 340 nm. A molar extinction coefficient of 6220 M^{-1} cm^{-1} for NADPH at 340 nm was used in the calculations. Phosphorylase activity in the direction of glycogen synthesis was measured at 30° and pH 6.8 with 5 µg/ml of enzyme, 1 mM AMP, 1% of glycogen, at a range of concentrations of Glc1*P* (3–20 mM) and inhibitor (1–5 mM) in 20 mM β-glycerophosphate, 1.5 mM EDTA, and 1 mM DTT buffer. The enzyme was preincubated with glycogen for 15 min at 30° before the reaction was started by adding Glc1*P*. Inorg. phosphate released in the reaction was determined, and initial reaction rates were calculated from the pseudo-first-order reaction constants as described [30]. Kinetic data were analysed by the use of the nonlinear regression program GraFit [31].

Crystallization and Data Collection. Native T-state GP*b* crystals were grown as described [32] in a medium consisting of 27–28 mg/ml of GP*b*, 1 mM spermine, 3 mM DTT, 10 mM BES, 0.1 mM EDTA, and 0.02% of sodium azide (pH 6.7, 16°). The crystals belong to the tetragonal space group $P4_32_12$ ($a = b = 128.5$ Å, $c = 116.3$ Å), with a single phosphorylase monomer in the asymmetric unit. Just before data collection, crystals were soaked in a soln. containing 5 mM triazole **3**, 50 mM sodium dihydrogenphosphate, 10 mM BES, 0.1 mM EDTA, and 0.02% of sodium azide at pH 6.7 for 1 h. Crystals were then transferred to 10 mM BES, pH 6.7, soln. containing 5 mM triazole, 50 mM sodium dihydrogenphosphate, and 25% of MPD as a cryoprotectant and soaked for a few seconds prior to mounting in a loop (made out of a single angora wool fibre) and flash frozen with an *Oxford-Cryosystems* cooling device operating with N_2 gas at 100 K. There were small changes in unit-cell dimensions on cooling, resulting in volume changes of 3–4% compared with native crystals from which data were collected at r.t. Data were collected from a single crystal of GP*b* prepared as above using a 18-cm diameter *MAR Research* image plate system which was mounted on the beamline X-ray diffraction (λ 1.0 Å) at *ELETTRA*, Trieste, Italy. The crystal to detector distance was set at 163 mm to give a maximum resolution of 2.0 Å at the edge of the detector. Reflections were indexed and integrated with the program DENZO [33] and were scaled using SCALEPACK [33]. Subsequent calculations were carried out using the CCP4 package [34].

Structure Refinement. Refinement of the [GP*b*-triazole-phosphate] complex was performed with XPLOR [35]. A set of reflections (10%) were held aside before refinement to monitor a free *R* factor [36]. The starting structure was the 2.4-Å-refined structure of the T state [GP*b*-tetrazole-phosphate][12] (*PDB* code: 1NOJ) comprising residues 14 to 842 and 389 H_2O molecules and with tetrazole and phosphate removed. Rigid body (15 steps), least squares conjugate gradient refinement (100 cycles, tolerance 0.05 Å) and restrained individual *B* factor refinement (60 cycles, target standard deviations of 1.5 $Å^2$ for 1–2 atom pair and 2.0 $Å^2$ for angle atom pairs) followed by simulated annealing, heating the structure to 3000 K and cooling to 300 K with a time step of 0.25 fs and a total time 0.7 ps resulted in a drop in *R* value from an initial 41.8% to 21.6%. At this stage, difference *Fourier* maps were calculated with SIGMAA-weighted ($F_o - F_c$) and ($2F_o - F_c$) coefficients [37] and the structure analysed with O [38]. Using PEAKMAX (from the CCP4 suite of programmes [34]), the ($F_o - F_c$) map was searched for peaks greater than 3.5 σ. The difference density indicated binding of triazole and phosphate at the catal. site and phosphate at the allosteric site. The maps also indicated that the side chain of Arg-309 had shifted into the allosteric site in order to contact the phosphate. A model of the triazole **3** [1] was fitted to the density at the catal. site, as was phosphate at both catal. and allosteric sites. Further H_2O molecules were determined and the peaks screened for likely H-bonds. A total of 111 new H_2O molecules were added to the model making a total of 500.

Several side chains and some main-chain atoms were adjusted, and refinement was continued with simulated annealing, heating the structure to 1000 K, and cooling to 300 K with a time step of 0.25 fs and a total time 0.7 ps, further conjugate gradient minimization (40 cycles), overall *B* factor refinement (15 cycles), and restrained *B* factor refinement (20 cycles) to give an *R* value of 20.3%. The free *R* value, used as a statistical cross-validation diagnostic for assessing improvement during refinement, fell to 27.6%. The X-ray data collection statistics and refinement results are shown in *Table 3*. Estimates of the precision of coordinates taken from previous studies indicate errors of the order of 0.2 Å [15]. The average *B* factors for main and side-chain atoms and H_2O molecules were 34, 36, and 40 Å, resp. Residues where *B* factor values exceeded 60 Å^2 included 14–22, 210–211, 250–262, 313–325, 554–556, and 831–842. A correction for the bulk solvent was not applied, and the low-resolution cutoff was 8 Å. The omission of low-resolution terms may account for the low electron density for parts of the molecule noted as being poorly ordered. However, these same residues are also poorly ordered in the structure of the native enzyme where low-resolution terms and a bulk-solvent correction were included in the refinement [15].

Table 3. *Statistics of Data Collection, Processing, and Refinement for [GPb]-Triazole-Phosphate] Complex*[a])

Cell dimensions	$a = b = 126.72$ Å, $c = 115.59$ Å
No. of reflections measured	271090
No. of unique reflections	37906
Resolution	15–23 Å
Completeness (outer shell 2.34–2.30 Å)	89.8% (76.1%)
$\langle I/\sigma(I)\rangle$ (outer shell 2.34–2.30 Å)	9.4 (2.9)
$R_m(I)$ (outer shell 2.34–2.30 Å)	0.097 (0.258)
No. of reflections used in refinement (8.0–2.3 Å, $F > 2\sigma$)	35849
No. of protein atoms	6757
No. of H_2O molecules in final cycle	500
No. of ligand atoms	24
Initial *R* factor (R_{free}) [%]	41.8 (42.0)
Final *R* factor (R_{free}) [%]	0.203 (0.276)
R.m.s. deviation in bond lengths	0.008 Å
R.m.s. deviation in bond angles	1.44°

[a]) Merging R_m is defined as $R_m = \sum_i\sum_h|\langle I_h\rangle - I_{ih}|/\sum_i\sum_h I_{ih}$, where $\langle I_h\rangle$ and I_{ih} are the mean and the *i*th measurement of intensity for reflection *h*, respectively. $\sigma(I)$ is the standard deviation of *I*. Crystallographic *R* factor is defined as $R = \sum\,||F_o| - |F_c||/\sum|F_o|$, where $|F_o|$ and $|F_c|$ are the observed and calculated structure-factor amplitudes, respectively. R_{free} is the corresponding *R* value for a randomly chosen 10% of the reflections that were not included in the refinement.

Analysis of Structure. The structure was analysed, and H-bonds were assigned if the distance between the electronegative atoms was less than 3.3 Å and if both angles between these atoms and the preceding atoms were greater than 90°. *Van der Waals* contacts were noted for non-H-atoms separated by less than 4 Å. Superposition of structures was performed with the least-squares option in O [38].

REFERENCES

[1] T. D. Heightman, M. Locatelli, A. Vasella, *Helv. Chim. Acta* **1996**, *79*, 2190.
[2] P. Ermert, A. Vasella, *Helv. Chim. Acta* **1991**, *74*, 2043.
[3] K. Tatsuta, Y. Ikeda, S. Miura, *J. Antibiot.* **1996**, *49*, 836.
[4] T. Granier, N. Panday, A. Vasella, *Helv. Chim. Acta* **1997**, *80*, 979.
[5] P. Ermert, A. Vasella, M. Weber, K. Rupitz, S. G. Withers, *Carbohydr. Res.* **1993**, *250*, 113.
[6] J. Sakon, W. S. Adney, M. E. Himmel, S. R. Thomas, P. A. Karplus, *Biochemistry* **1996**, *35*, 10648.
[7] W. P. Burmeister, S. Cottaz, H. Driguez, R. Iori, S. Palmieri, B. Henrissat, *Structure* **1997**, *5*, 663.
[8] C. Wiesmann, W. Hengstenberg, G. E. Schulz, *J. Mol. Biol.* **1997**, *269*, 851.
[9] G. Papandreou, M. K. Tong, B. Ganem, *J. Am. Chem. Soc.* **1993**, *115*, 11682.

[10] K. Tatsuta, S. Miura, S. Ohta, H. Gunji, *Tetrahedron Lett.* **1995**, 1085.
[11] T. D. Heightman, P. Ermert, D. Klein, A. Vasella, *Helv. Chim. Acta* **1995**, *78*, 514.
[12] E. P. Mitchell, S. G. Withers, P. Ermert, A. T. Vasella, E. F. Garman, N. G. Oikonomakos, L. N. Johnson, *Biochemistry* **1996**, *35*, 7341.
[13] P. J. McLaughlin, D. I. Stuart, H. W. Klein, N. G. Oikonomakos, L. N. Johnson, *Biochemistry* **1984**, *23*, 5862.
[14] H. W. Klein, M. J. Im, D. Palm, *Eur. J. Biochem.* **1986**, *157*, 107.
[15] K. R. Acharya, D. I. Stuart, K. M. Varvill, L. N. Johnson, 'Glycogen Phosphorylase: Description of the Protein Structure', World Scientific Publishers, Singapore–London, 1991.
[16] L. N. Johnson, J. Hajdu, K. R. Acharya, D. I. Stuart, P. J. McLaughlin, N. G. Oikonomakos, D. Barford, 'Allosteric Enzymes', Ed. G. Herve, CRC Press Inc., Boca Raton, Florida, 1989, pp. 81–127.
[17] L. N. Johnson, *FASEB J.* **1992**, *6*, 2274.
[18] N. G. Oikonomakos, K. R. Acharya, L. N. Johnson, 'Post-translational Modifications of Proteins', Eds. J. J. Harding and M. J. C. Crabbe, CRC Press Inc., Boca Raton, Florida, 1992, pp. 81–151.
[19] N. G. Oikonomakos, K. R. Acharya, D. I. Stuart, A. E. Melpidou, P. J. McLaughlin, L. N. Johnson, *Eur. J. Biochem.* **1988**, *173*, 569.
[20] L. N. Johnson, K. R. Acharya, M. D. Jordan, P. J. McLaughlin, *J. Mol. Biol.* **1990**, *211*, 645.
[21] Semichem, 'AMPAC 5.0', 7128 Summit, Shawnee, KS 66216, 1994.
[22] J. Conchie, G. A. Levvy, *Biochem. J.* **1957**, *65*, 389.
[23] T. Niwa, S. Inouye, T. Tsuruoka, Y. Koaze, T. Niida, *Agric. Biol. Chem.* **1970**, *34*, 966.
[24] R. Hoos, A. B. Naughton, W. Thiel, A. Vasella, W. Weber, K. Rupitz, S. G. Withers, *Helv. Chim. Acta* **1993**, *76*, 2666.
[25] G. Papandreou, M. K. Tong, B. Ganem, *J. Am. Chem. Soc.* **1993**, *115*, 11682.
[26] E. J. M. Helmreich, C. F. Cori, *Proc. Natl. Acad. Sci. U.S.A.* **1965**, *51*, 131.
[27] E. H. Fischer, E. G. Krebs, *Methods Enzymol.* **1962**, *5*, 369.
[28] A. E. Melpidou, N. G. Oikonomakos, *FEBS Lett.* **1983**, *154*, 105.
[29] L. L. Kastenschmidt, J. Kastenschmidt, E. Helmreich, *Biochemistry* **1968**, *7*, 3590.
[30] N. G. Oikonomakos, M. Kontou, S. E. Zographos, K. A. Watson, L. N. Johnson, C. J. F. Bichard, G. W. J. Fleet, K. R. Acharya, *Protein Sci.* **1995**, *4*, 2469.
[31] R. J. Leatherbarrow, 'GraFit Version 3.0'., Erithakus Software, Staines, UK, 1992.
[32] N. G. Oikonomakos, A. E. Melpidou, and L. N. Johnson, *Biochem. Biophys. Acta* **1985**, *832*, 248.
[33] Z. Otwinowski, 'DENZO. Data Collection and Processing, DL/SC1/R34', SERC Laboratory, Darcsbury, Warrington, UK, 1993.
[34] Collaborative Computational Project, Number 4, 'The CCP4 Suite: Programs for Protein Crystallography', *Acta Crystallogr., Sect. D* **1994**, *50*, 760.
[35] A. T. Brunger, 'X-PLOR Version 3.1. A System for X-Ray Crystallography and NMR', Yale University Press, New Haven–London, 1992.
[36] A. T. Brunger, *Nature (London)* **1992**, *355*, 472.
[37] R. J. Read, *Acta Crystallogr., Sect. A* **1986**, *42*, 140.
[38] T. A. Jones, J. Y. Zou, S. W. Cowan, M. Kjeldgaard, *Acta Crystallogr., Sect. A* **1991**, *47*, 110.

Received January 26, 1998